# Quasi-unidirectional flax composite reinforcement: Deformability and complex shape forming

B. Vanleeuw [a], V. Carvelli [b,*], M. Barburski [c], S.V. Lomov [a], Aart W. van Vuure [a]

[a] Department of Materials Engineering, K. U. Leuven, Kasteelpark Arenberg 44, 3001 Leuven, Belgium
[b] Department of Architecture, Built Environment and Construction Engineering, Politecnico di Milano, Piazza Leonardo Da Vinci 32, 20133 Milan, Italy
[c] Institute of Architecture of Textile, Technical University of Lodz, Zeromskiego 116, 90-924 Lodz, Poland

Received 2 September 2014
Received in revised form 15 January 2015
Accepted 31 January 2015
Available online 7 February 2015

## 1. Introduction

In any composite manufacturing process a crucial step is the forming of the initial planar reinforcement into a desired three-dimensional shape. After shaping, the formed reinforcement is impregnated with resin and consolidated. In the forming process, the deformability of the reinforcement plays a key role in definition of the fibres' orientations, which influences permeability of the preform and finally defines the mechanical performance of the composite component [1,2]. Therefore, the knowledge of the deformation behaviour of a dry composite reinforcement is important to predict and avoid defects (e.g. wrinkles) in complex preform shapes.

Focusing on continuous fibre materials, the investigations available in the literature [1,2] are mainly dedicated to the deformability and formability of textile reinforcements with 2D interlacements, and recently of textiles with 3D architectures ([3–6]), made of synthetic fibres (i.e. glass, carbon, etc.).

In the last decade the interest in environmentally friendly composites has been rapidly increased. Several works have been published on research dealing with natural fibres, bio-based matrices and their composites (e.g. [7–13]). Natural fibres are particularly attractive for several reasons: they are very popular and abundant in developing countries; they have low cost compared to synthetic fibres; they have good specific mechanical properties and good acoustic or vibrational damping. Moreover, the energy needed for production of natural fibres is much lower than for synthetic fibres and, at last, life cycle analysis (LCA) studies strongly support further development of biomaterials [14]. The main disadvantages of natural fibres as reinforcement of composites are the compati-bility between fibre and matrix and their relatively high moisture absorption [11]. In spite of the fast growing interest for natural fibres in the composites industry, the deformability and formability behaviour of natural fibre fabrics as reinforcement are not deeply known and investigated. Only recently, in the authors' knowledge, few investigations on the mechanical properties and complex shape forming of flax woven fabrics have been published ([15–17]).

In this paper, the deformability and formability of a flax fabric adopted as reinforcement in manufacturing complex shape composite components are experimentally investigated. The fabric (commercialized as FLAXPLY UD 180 by LINEO) is a quasi-unidirectional woven fabric with thin twisted weft yarns connecting thick warp yarns using a weft rep weave interlacing pattern. The unbalanced nature of the quasi-unidirectional weave presents additional challenges to the fabric forming [18].

The first part of the study is focused on the measurement of the main deformation mechanisms of the fabric involved in shaping processes: in-plane uniaxial and biaxial tension; in-plane shear; out-of-plane bending and out-of-plane compression. Particular attention is dedicated to the deformation during shear loading, this

* Corresponding author. Tel.: +39 0223994354.
*E-mail address:* valter.carvelli@polimi.it (V. Carvelli).

being considered the primary deformation mechanism in reinforcement shaping processes [19]. The tests are assisted by the 2D digital image correlation (DIC) technique to have a continuous measurement of the local deformations on the fabric surface. The peculiarities of the deformation behaviour are highlighted and connected to the quasi-unidirectional construction of the flax fibre fabric.

The second part is dedicated to the experimental study of a complex 3D shape forming process. The drapability of the quasi-unidirectional flax reinforcement was observed using a double-dome punch in an open die forming process. The tests are assisted by 3D digital image correlation technique to have a continuous measurement of the local deformation during shaping, in particular of the shear deformation.

The obtained results represent a complete data set for characterisation of the deformation capabilities of the quasi-unidirectional flax reinforcement during complex 3D shape forming processes and provide benchmarking data for numerical predictions. Based on the present results, in future work available numerical modelling approaches (e.g. [20–22]) can be adopted to predict the forming process of complex shapes assuming the knowledge of the main mechanical features of the quasi-unidirectional flax reinforcement, as described in Section 4, and assessing the accuracy with the experimental forming results presented in Section 5. This investigation can increase the confidence in adopting the flax fibre quasi-UD reinforcement instead of or beside to synthetic fibre woven fabrics in forming complex composite shapes without undesirable defects.

## 2. Material

The fabric is a quasi-unidirectional flax reinforcement (commercialized as FLAXPLY UD 180 by LINEO). The fibres architecture of the preform has 95.5% of the fibres (by weight) in warp direction and 4.5% in weft. The flax fibre density is 1.4 g/cm$^3$. The fabric has a weft rep weave 4/4(4), i.e. each weft yarn goes up and under 4 warp yarns (see Fig. 1). Some measured features of the reinforce-ment are listed in Table 1.

## 3. Experimental methodologies and devices

Biaxial tensile tests at different velocity ratios at two axes were performed to gather information on the initial non-linear stiffening due to the very low crimp in the tows, while uniaxial bias extension and picture frame tests were carried out to experimentally determine the in-plane shear behaviour of the flax preform. During these tests, images were recorded by a digital camera for image correlation analysis by Vic-2D software [23]. For this purpose the specimen surface was speckled with black acrylic paint for strain components measurements with a digital image correlation system [24]. The procedure followed for image analysis is detailed in [25].

**Table 1**
Measured properties of the quasi-unidirectional flax reinforcement.

| | | |
|---|---|---|
| | Fabric plies | 1 |
| | Areal density (g/m$^2$) | 180 |
| Warp | Insertion density (ends/cm) | 42.5 |
| | Linear density of yarns (tex) | 41.6 |
| Weft | Insertion density (picks/cm) | 3 |
| | Linear density of yarns (tex) | 27.7 |

Out-of-plane deformability behaviour was investigated with bending and compression tests.

Bending stiffness of a textile plays an important role in its drapability [26] and transverse compression is one of the main deformation modes [27] during the compaction stage of resin infusion processes due to the applied vacuum and possible additional pressure, which modifies the final material thickness.

Furthermore, the forming stage using a complex double curvature mould was experimentally investigated for two orientations of the fibres, assuming a punch with double-dome shape and measuring the full field displacement with three dimensional image correlation analyses by MatchID3D software [28].

The tests were performed in the labs of Politecnico di Milano and KU Leuven.

### 3.1. Biaxial tension tests

Biaxial and uniaxial tension tests were performed on square specimens of the fabric, using a biaxial testing machine in KU Leuven equipped with two independent orthogonal axes (Fig. 2), with grips of length 190 mm. Velocity of the two loading axes was set in the range 1–2 mm/min to have different warp to weft velocity ratios ($k$ = warp velocity/weft velocity). It should be underlined that the velocity ratio (imposed by the device) does not coincide with the strain ratio in the centre of a specimen under biaxial loading. Four load cells of 5 kN were used to measure the force applied to each side of the specimen. During testing, a digital camera acquired frames at a frequency of 1 Hz for image post-processing. The biaxial tension test set up is illustrated in Fig. 2.

### 3.2. In-plane shear behaviour

Two tests are generally performed for in-plane shear characterisation of engineering fabrics, namely uniaxial bias extension and picture frame test (see e.g. [2,29]). Most of the studies concerning shear testing of fabrics ([29,30]) include normalization procedures for the bias force, based on the energy approach proposed by Harrison et al. in [30]. The normalization procedures provide the

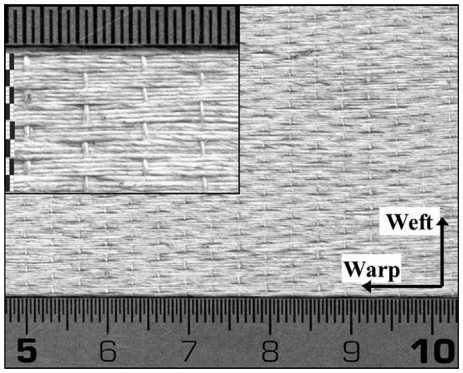


**Fig. 1.** Quasi-unidirectional flax reinforcement (LINEO – FLAXPLY UD 180).

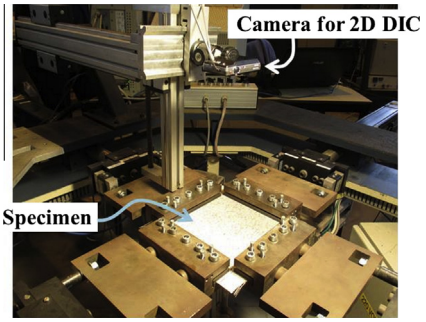


**Fig. 2.** Uni/biaxial tension test. Biaxial tensile machine and test set-up.

intrinsic shear behaviour of fabrics and allow a comparison between bias extension and picture frame results.

In the present work, uniaxial bias extension and picture frame tests are compared using the normalization procedures detailed in [31,32] and [29,33], respectively.

During shear tests a digital camera acquired frames at a frequency of 1 Hz, for the measurement of the local shear angle by digital image correlation. The local shear angle evaluation follows the procedure detailed in [33] based on the coordinates of the corners of the facets (initially square), virtually imposed on the textile surface, extracted on each image by the software Vic-2D [23].

*3.2.1. Uniaxial bias extension test*

Uniaxial bias extension tests involve rectangular specimens of material with warp and weft directions of the tows orientated initially at ±45° to the direction of the applied tension load. The specimen is characterized by the free length/width ratio ($\lambda = L_o/w_o$), where the total free length ($L_o$) must be at least twice the width ($w_o$), in order to guarantee a pure shear zone in the centre of the specimen (see e.g. [34]) assuming yarns being inextensible and no slip occurs in the sample [32]. When the length/width ratio ($\lambda$) of the bias extension specimen is at least 2, the shear angle ($\gamma$) in the centre zone should obey the kinematic relationship in Eq. (1), as long as deformation mechanisms, such as intra-ply slip, are insignificant compared with trellis shearing [35]. Eq. (1) corre-lates the shear angle ($\gamma$) to the fabric geometry (length of the undeformed centre zone $D$) and the end displacement ($d$).

$$\gamma = \frac{\pi}{2} - 2\cos^{-1}\left(\frac{D+d}{D\sqrt{2}}\right) \quad (1)$$

Glass fibre–epoxy tabs 2 mm thick, 100 mm wide and 65 mm long were glued at the ends of the fabric specimens, leaving 200 mm free length between the grips, which gives a length/width ratio ($\lambda$) of 2 (Fig. 3). A tensile machine (Instron 5567) was used with a load cell of 1 kN. A test speed of 5 mm/min was imposed.

*3.2.2. Picture frame test*

The picture frame shear test consists in clamping a fabric on a hinged frame whose directions are those of the fabric yarns [36]. In the present study the setup available in KU Leuven (see Fig. 4a) was used (see e.g. [29]). The lack of an official standard for picture frame test leads to difficulties in comparing the results of different test labs. The test has been the subject of a benchmark exercise to try to homogenize the results [29]. The procedure used in this work follows the "best practice" recommendations of [29].

Fig. 4a shows the adopted picture frame. The shear angle of the frame ($\gamma$) is related to the displacement of the machine as detailed in [29,33].

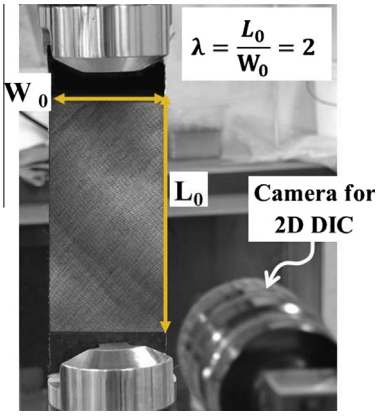


**Fig. 3.** Bias extension test: test set-up.

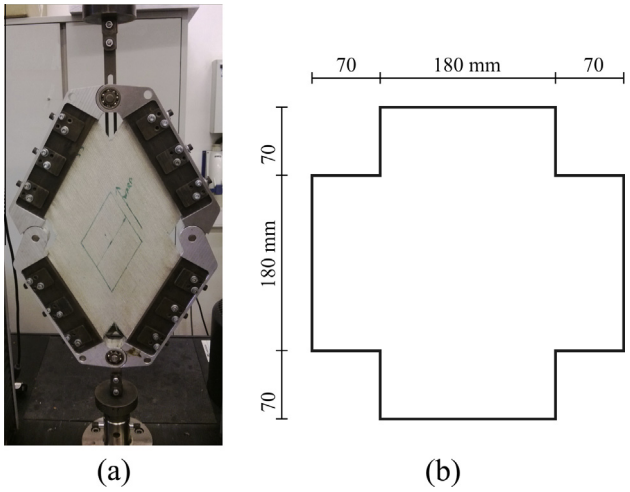


**Fig. 4.** Picture frame: (a) set up; and (b) specimen geometry.

The frame was mounted on an Instron 5567 tensile machine with 1 kN load cell. A test speed of 20 mm/min and a maximum displacement of 22 mm, corresponding to a frame shear angle of ≈50°, were set. First, the load–displacement diagram was registered with the empty frame, to be subtracted from the load diagram in the test with the fabric, to produce the net force applied by the machine. The basics of the picture frame kinematics, as well as the calculation procedures for the shear force, are detailed in [25]. The tested samples had the cross-like shape depicted in Fig. 4b.

*3.3. Out-of-plane bending test*

Two test methods are adopted to measure the bending stiffness of fabrics [37]: a cantilever bending test, which originates from the work of Peirce [38] (see standard [39]) and the Kawabata test [40]. In the following, bending tests in warp and weft direction of the reinforcement are detailed using the same type of flexometer as the one described in [41]. The device consists of a metallic part, which enables to place the sample in cantilever configuration bending under its own weight (Fig. 5) and an optical device acquir-ing images of the bent specimen. The quasi-static bending tests with different overhanging lengths allow to measure the non-lin-ear moment vs. curvature relationship. After each length incre-ment and before taking an image of the deformed configuration, the reinforcement relaxes for five minutes reaching a 'stable' configuration. The image processing generates digital profiles of bent specimens adopted for curvature and moment evaluations. The samples had width of 50 mm.

*3.4. Out-of-plane compression test*

The response of the reinforcement in terms of thickness variation is an important knowledge for the preliminary prediction of

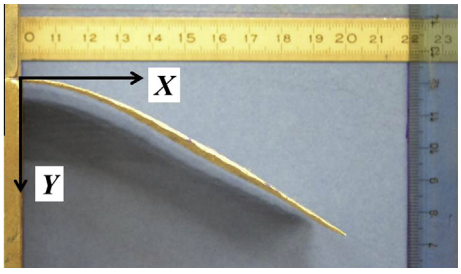


**Fig. 5.** Bending test set up.

the fibre content in the composite component and, as consequence, of the mechanical properties. The thickness of the considered fabric during transverse compression was experimentally measured with a set-up similar to the one detailed in [42]. It consists of a metallic cylindrical punch of diameter 70 mm applying compressive pressure, and a metal frame for specimen positioning. A spherical hinge was adopted to uniformly distribute the pressure on the contact surface reducing the possible slight error of parallelism between the punch and textile plane. The compression test set-up is illustrated in Fig. 6a; while the sample geometry is depicted in Fig. 6b.

First a calibration curve is recorded in a compression test without specimen to account for the machine compliance. After calibration, fabric specimens are inserted and clamped in the frame.

For each specimen three load–unload cycles were performed. The thickness vs. pressure diagram was deduced subtracting the calibration curve from the load–displacement data of each specimen.

An Instron 5567 machine, with a load cell of 1 kN was used. The maximum applied pressure in each cycle was 250 kPa.

### 3.5. Forming test

The forming process was investigated with the test set-up illustrated in Fig. 7. It consists of two modules: a set of metal components and optical devices. The first module is made up of a punch with double-dome shape, a metal open die on which the composite reinforcement is placed and a rectangular blankholder. The double-dome punch was the one introduced in the benchmark study [43] and was also used in [44]. The geometry of the metal tools is depicted in Fig. 8. The optical module is a stereo vision sys-tem (see Fig. 7), which acquires images of the forming process at a frequency of 1 Hz for 3D image correlation analysis by MatchID3D software [28]. For this purpose the specimen surface is speckled with black acrylic paint for displacement measurements with dig-ital image correlation technique. A rectangular blank (500 × 400 mm) is placed on the die and then the punch is pushed down at a constant rate of 10 mm/min. The test continues until the forming process is finished, i.e. the punch passes entirely through the die (approximately 55 mm of punch displacement).

## 4. Results of deformability tests

### 4.1. Biaxial tensile behaviour

Fig. 9 summarizes the results of the uniaxial tension test in warp and weft direction, as well as biaxial tension in the principal

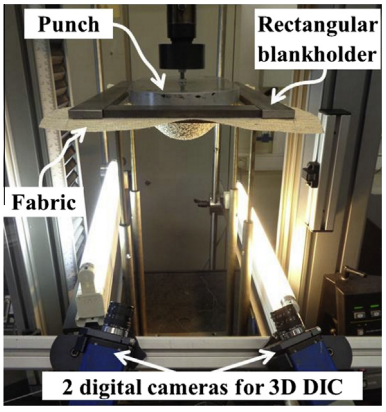


**Fig. 7.** Forming test set up of double-dome shape.

directions. Each curve in Fig. 9 is the average of three/four specimens. The biaxial tests were performed with four different velocity ratios $k$ (warp/weft).

The force levels when tested in the weft direction are considerably lower, which is a logical consequence of the warp/weft distribution of the yarns in the fabric. The reinforcement shows a larger non-linear range in the weft direction, which is probably related to two aspects: the higher crimp of the weft yarns which gives the main non-linear contribution, and the weft yarn twist which contribution is relatively small observing the initial limited nonlinear behaviour during tensile tests of yarns extracted from the fabric. When tested in warp direction, the behaviour is less sensitive to the tension applied in the weft direction (see Fig. 9a), with the biaxial curves close to each other ($k$ = 1/1, 1/2, 1/0, 2/1). This is probably again related to the low weft yarn density and the non-linear behaviour of the weft yarns. However, when comparing the biaxial test results with the unconstrained sample, it is remarkable that the introduction of tension in the weft direction causes a strong reduction in initial strain in the warp direction.

Fig. 9a shows a reduced experimental scatter for loading in warp direction. The curves, after the initial non-linear range, become approximately linear with slope close to the one of the uniaxial tension. The maximum slope of the curves obtained by biaxial and uniaxial tensile tests represents almost the stiffness of the adopted flax yarns. In fact, assuming a flax density 1.4 g/cm$^3$, the data of the yarns in Table 1, the maximum slope of each curve in warp direction and the theoretical cross section of the warp yarns, the obtained stiffness is in the range 15.6–18.8 GPa. The stiffness of 24 flax yarns extracted from the fabric in warp

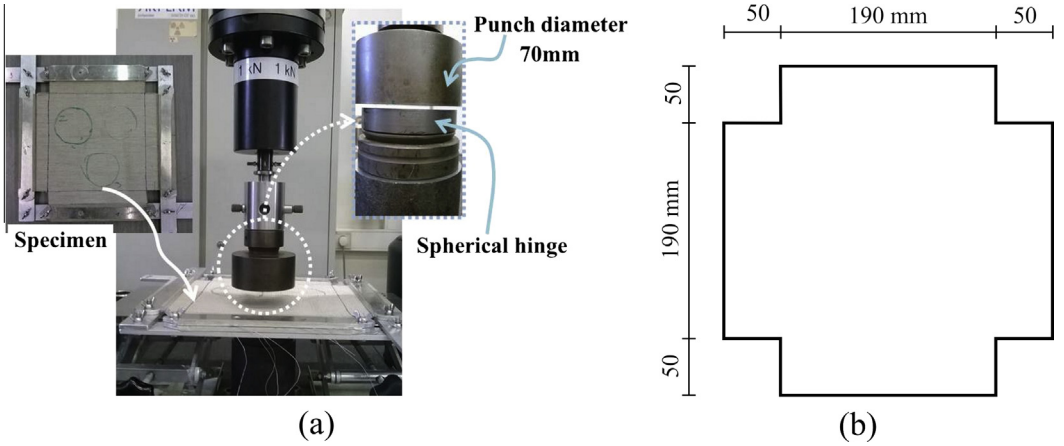


**Fig. 6.** Compression test: (a) set-up; and (b) specimen geometry.

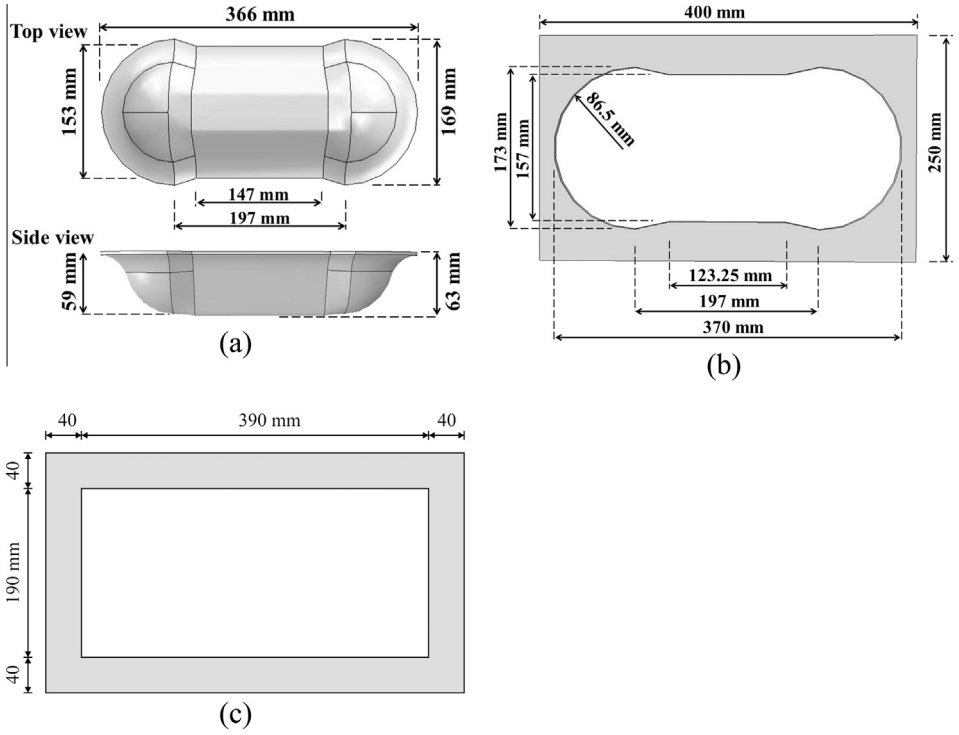


**Fig. 8.** Geometry of (a) double-dome punch, (b) open die (thickness 8 mm) and (c) blankholder (thickness 4 mm).

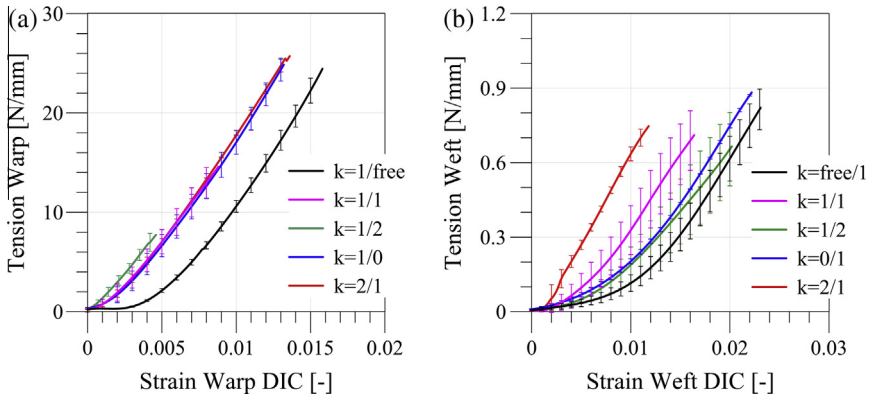


**Fig. 9.** Uniaxial and biaxial tests. Average tension vs. strain curves in (a) warp and (b) weft direction for different ratios $k$ ($k$ = warp/weft velocity); $k$ = 1/free and $k$ = free/1 denote uniaxial tests in the warp and weft directions. Error bars give the standard deviation of three/four tests.

direction was measured by tensile tests. The adopted free length of 200 mm and the theoretical cross section allow having an average stiffness of the warp yarn of 17.4 GPa.

A larger experimental scatter is observed for loading in weft direction (Fig. 9b). This is mainly due to the reduced number of yarns in weft direction and the relatively low applied loads. The stiffness of the fabric in weft direction slightly increases with increase of $k$, due to the tensioning effect of the large fraction of warp yarns.

### *4.2. In-plane shear behaviour*

The assumptions of the normalization procedure adopted for bias tension, presented in Section 3.2.1, have been assessed for several 2D reinforcements (see e.g. benchmark in [29]). These hypotheses are now verified for the quasi-uniaxial heavily unbalanced flax fabric under consideration.

The comparison of the local shear angle measured by DIC in the centre of five specimens during bias tests, and the theoretical shear angle, calculated based on kinematic analysis (Eq. (1)), is detailed in Fig. 10a. The measured and the theoretical shear angles are in agreement in the considered range with an underestimation of the DIC lower than 3° for shear angle above 30°. Analogous information is obtained comparing the measured shear angle in the centre of the specimen to the frame shear angle of five picture frame tests (Fig. 10b). The frame shear angle is related to the displacement of the machine and to the kinematics of the picture frame; it does not contain assumptions on the deformation mechanism of the fabric. In Fig. 10b the difference between the nominal and DIC-measured shear angle is negligible (less than 2°).

The measured shear angle distribution on the complete surface (200 × 100 mm) of a bias specimen for an applied theoretical shear angle of ≈20° is depicted in Fig. 11a. The assumption of the kinematic model (see e.g. [34]), i.e. distinction of three deformation

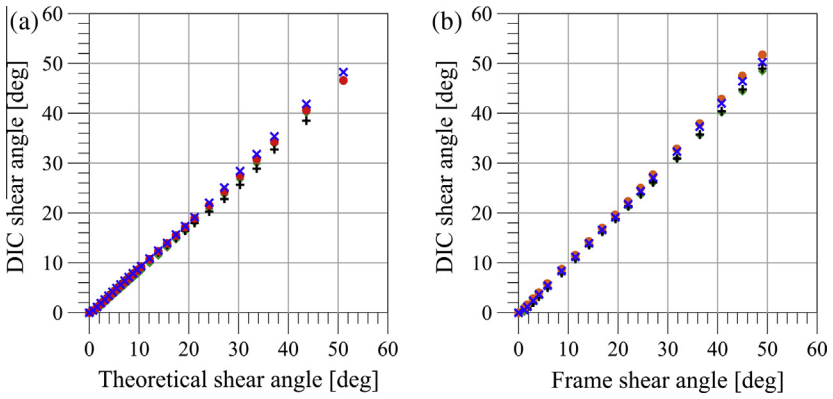


**Fig. 10.** Comparison of measured and theoretical shear angle of five: (a) bias extension tests and (b) picture frame tests.

zones, is clearly observed in the experiments. Moreover, the shear angle distribution in the centre of a picture frame specimen under the theoretical shear angle of ≈20° is detailed in Fig. 11b. The picture shows shear angles in the range 18–22°.

The average normalized shear force vs. DIC shear angle curve of five specimens subjected to bias extension is depicted in Fig. 12 and compared to the one obtained with five picture frame tests. The diagram shows the curves, measured with two different tests, very close to each other and in the same experimental scatter band for a large shear angle range up to 40°.

The good agreement of the shear curves obtained with the two different tests is not frequently observed in the literature. It is usual to have a discrepancy of the test results due to the different clamping of the specimen in the two test setups ([25,30]). The considered quasi-unidirectional flax reinforcement does not show a considerable influence of the specimen clamping on the shear behaviour, because of the interlacement of the quasi-UD fabric (highly unbalanced distribution of the fibres in the warp and weft direction) leading to a weak interaction during relative rotation of the fibres.

The observed shear behaviour of the quasi-UD fabric has some differences in comparison to several two-dimensional reinforcements for composites investigated in literature. It is usual to distinguish three different regions in the shear curve (e.g. [30,42]): an initial region of high initial stiffness, a second region of low shear stiffness and a third with a fast increase of the curves slope. These regions correspond to different shear resistance mechanisms and are well explained in the literature for two-dimensional fabrics

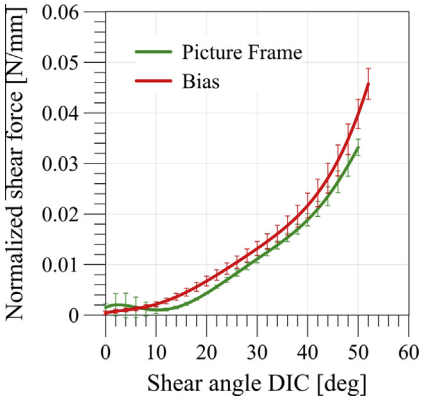


**Fig. 12.** Comparison of bias extension and picture frame tests: average normalized shear force vs. DIC shear angle curves. Error bars give the standard deviation of five tests.

(see e.g. [45,46]). For 2D textiles, the high initial stiffness originates from high resistance of the yarns to lateral bending, when they cannot rotate in the intersections, as the applied force does not exceed friction between them. When the friction has been overcome, it becomes the main force factor and low shear stiffness is observed. Increasing the shear angle, the yarns are coming closer to one another and start being compressed laterally. The compression of fibrous assemblies is a non-linear process with fast increasing stiffness, which explains the fast increase of the shear stiffness in the third stage of the deformation. The first region is not observed for

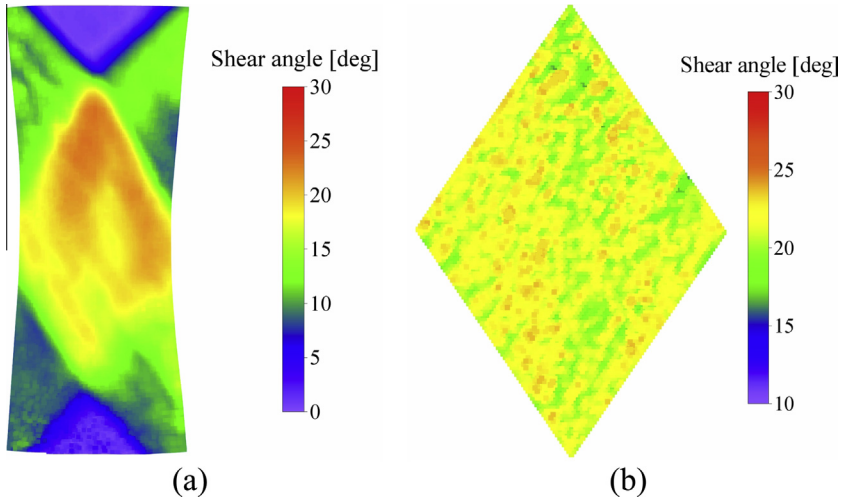


**Fig. 11.** Contour plot of the measured shear angle distribution by DIC for a theoretical shear angle of 20°. (a) Bias extension; and (b) picture frame.

the quasi-unidirectional flax reinforcement. The low quantity of yarns in weft direction generates few intersections between warp and weft yarns and as consequence the initial friction at the intersections does not play an important role in the initial shear behaviour. Up to a shear angle of almost 10° (Fig. 12), the flax yarns move closer to each other and the curves show negligible shear stiffness of the fabric. Then, the yarns start to be in contact and compressed laterally and the shear curves have a rapid non-linear increase of the slope. The contact of the yarns generates an initiation of wrinkles for a shear angle of about 20–23°, in both tests.

### 4.3. Out-of-plane bending behaviour

The average profiles of the bent specimens have been measured for different overhanging lengths by image post-processing (see Fig. 13). The bent profile of each specimen ($y(x)$) is fitted with a fourth order polynomial function. In Fig. 13, each curve in both warp and weft direction is the average of five tests. The curvature ($\kappa$) of the bent shape is calculated as:

$$\kappa(x) = \frac{y''}{(1+y'^2)^{\frac{3}{2}}} \tag{2}$$

where apex means the derivative of the deflection $y$ with respect to the coordinate $x$ (see Fig. 5).

The bending moment has been calculated with a digital method as in [6]. The image of the bent profile is subdivided in segments of length 0.5 mm. The weight per unit length and the distance of the centroid to the clamp give the contribution of each segment to the bending moment.

The curvature and the bending moment at the clamp for different overhanging lengths are summarized in Fig. 14a and b, respectively. Four and three overhanging lengths have been considered in warp (from 50 to 125 mm) and weft (from 20 to 40 mm) direction,

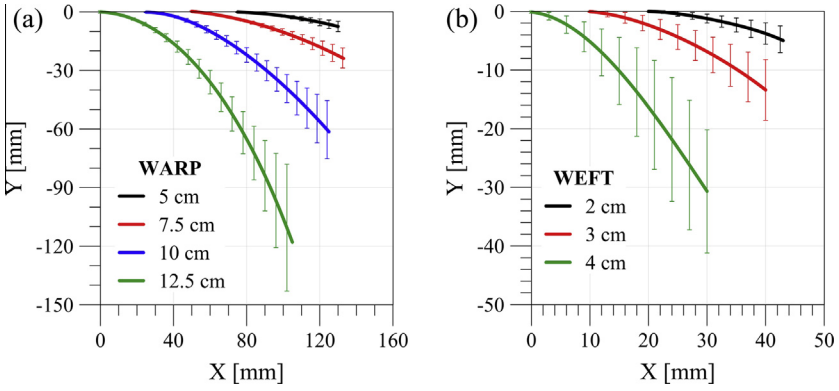


**Fig. 13.** Bending tests. Fourth order polynomial fitting of bent specimen average profiles extracted by images post-processing for different overhanging length, in: (a) warp and (b) weft direction. Error bars give the standard deviation of five tests.

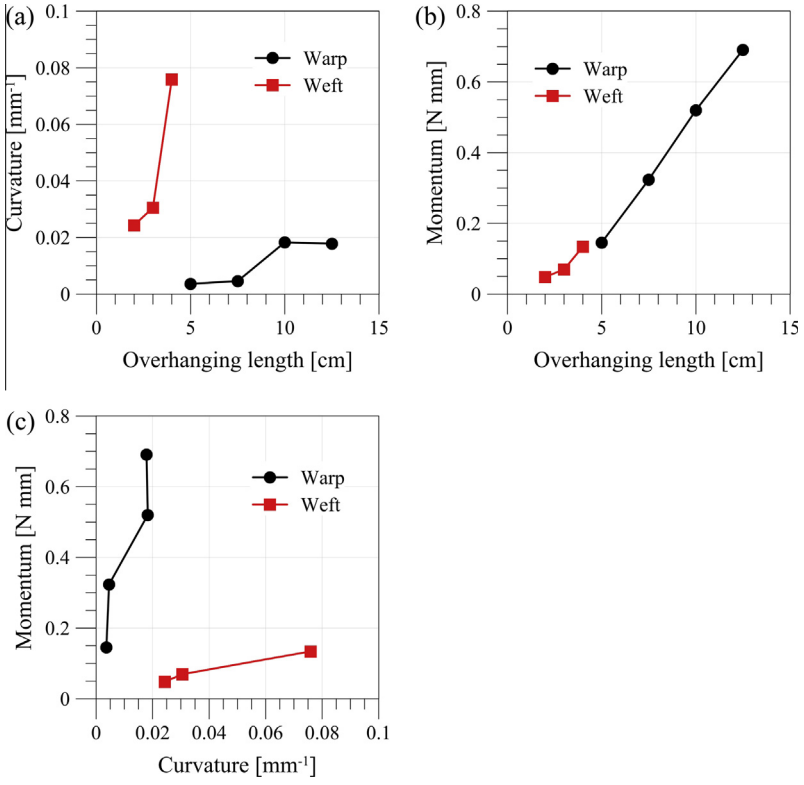


**Fig. 14.** Bending tests. (a) curvature vs. overhanging length; (b) bending moment vs. overhanging length; and (c) bending moment vs. curvature.

**Table 2**
Comparison of bending moment and curvature for the flax quasi-UD and two carbon textiles (Fabric A and Fabric B) adopted in [41], for an overhanging length of 125 mm.

| | Moment per unit width (N) | Curvature ($mm^{-1}$) |
|---|---|---|
| Fabric A – weft | 0.042 | 0.017 |
| Fabric B – weft | 0.045 | 0.011 |
| Flax quasi-UD – warp | 0.014 | 0.018 |

respectively. The combination of these results provides the moment–curvature curves of the flax reinforcement in Fig. 14c.

As expected, the highly unbalanced flax fabric has a completely different bending behaviour in the two principal directions. The higher density of warp yarns gives a higher bending stiffness of the fabric along this direction.

For the sake of comparison with fabrics of synthetic fibres, the bending moment and curvature measured with the flax quasi-UD fabric and two carbon textiles adopted in [41] are listed in Table 2 for an overhanging length of 125 mm. The carbon fabrics detailed in [41] are: a 2.5D carbon fabric 630 g/$m^2$ (named Fabric A) and an interlock carbon fabric 600 g/$m^2$ (named Fabric B). The compar-ison of the three reinforcements with different fibres (flax and car-bon) is not completely adequate. But, to the authors' knowledge, bending stiffness measurements of other flax reinforcements for composites are not available in literature. The quasi-UD fabric has almost one-third of the bending moment and similar curvature as the carbon reinforcements. As expected, the flax reinforcement reveals a lower bending stiffness compared to the considered car-bon textiles.

### *4.4. Out-of-plane compression behaviour*

The fabric thickness as function of the compaction pressure has been measured with six specimens.

Fig. 15a details the average diagrams recorded in three consec-utive compression quasi-static loading cycles. During the first loading, the fabric had preliminary compaction that remains per-manent, having almost identical curves for the second and third loading cycle. In the first cycle some handling and production vari-ations of the yarns position have been recovered.

The shape of the curves in Fig. 15a is characteristic for the com-paction behaviour of textiles (e.g. [47,48]). Three regions can be distinguished according to the deformation mechanisms. The first region features a low compressive rigidity. Here friction and bend-ing of yarns show low resistance while rearranging themselves inside the fabric structure. The second region, transition zone, is strongly non-linear. The contact points between yarns are increas-ing, creating a higher frictional and bending resistance. Lateral compression of adjacent yarns starts at some points. At last, the third region shows an almost asymptotic behaviour of the fabric where the compressive rigidity is very high. All yarns are in close contact and the lateral compression of the yarns features high compressive forces.

The importance in measuring the thickness variation during compaction is related to the preliminary prediction of the fibre vol-ume fraction of the composite material reinforced with the consid-ered fabric.

The fibre volume fraction ($V_f$) is estimated as $V_f = A/\rho h$, being $A$ the fabric areal density, $\rho$ the flax fibre density (1400 kg/$m^3$) and $h$ the measured fabric average thickness (assuming the thickness of the composite as the thickness of the fabric).

Fig. 15b shows the predicted fibre volume fraction vs. the applied pressure in the three loading cycles. Focussing the atten-tion on the first cycle, as for a possible infusion process, the fibre volume fraction ranges from 23.5% for a pressure of 1 kPa to 39.4% applying 250 kPa. In [49], fibre volume fraction of 47% was reached for laminates made of the same LINEO prepreg at a pres-sure of 400 kPa. These results are comparable to the data presented in [50] for a flax plain weave fabric and a flax non-crimped stitched unidirectional fabric which feature a fibre volume fraction in the range 40–50% after compression up to 250 kPa. It must be men-tioned that the obtained theoretical fibre volume fraction of 39.4% is for one layer of quasi-UD fabric. Generally, a composite laminate contains several layers and the applied pressure in the infusion process generates nesting of the yarns and, as conse-quence, an increase of the fibre volume fraction. This was observed by compression tests of four layers of the quasi-UD fabric. For a pressure of 250 kPa, the theoretical fibre volume fraction was almost 46%.

## 5. Results of formability tests

The drapability of the quasi-unidirectional flax reinforcement on complex double curvature moulds was experimentally investi-gated using a double-dome punch in an open die forming process (see details in Section 3.5).

Six tests were performed: three with warp yarns and three with weft yarns of the fabric initially aligned to the longer side of the rectangular open die (longitudinal direction).

Shear deformation is considered as one of the primary deforma-tion mechanisms in the forming of composite reinforcements [19]. The local shear angle is calculated by means of the 'grid method',

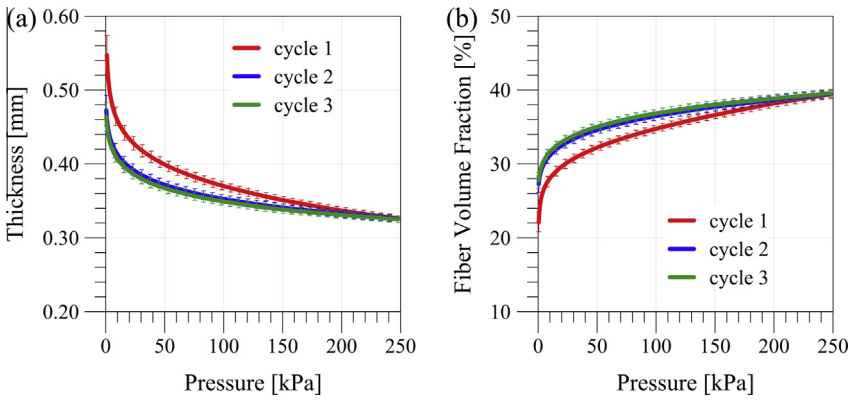


**Fig. 15.** Transversal compression tests. (a) Average fabric thickness vs. compaction pressure; and (b) prediction of fabric fibre volume fraction vs. compaction pressure. Error bars give the standard deviation of six tests.

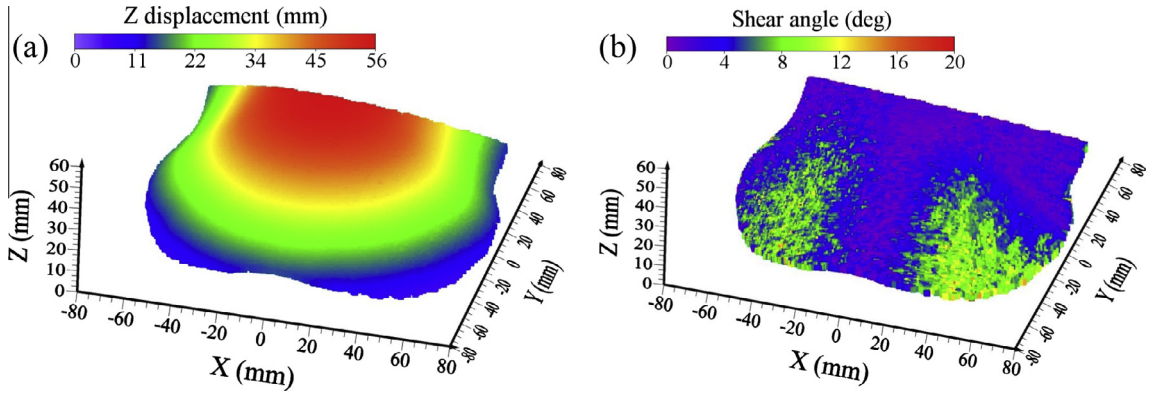


**Fig. 16.** (a) Displacement and (b) shear angle distribution at the end of forming process of double-dome shape with warp fibres in longitudinal direction.

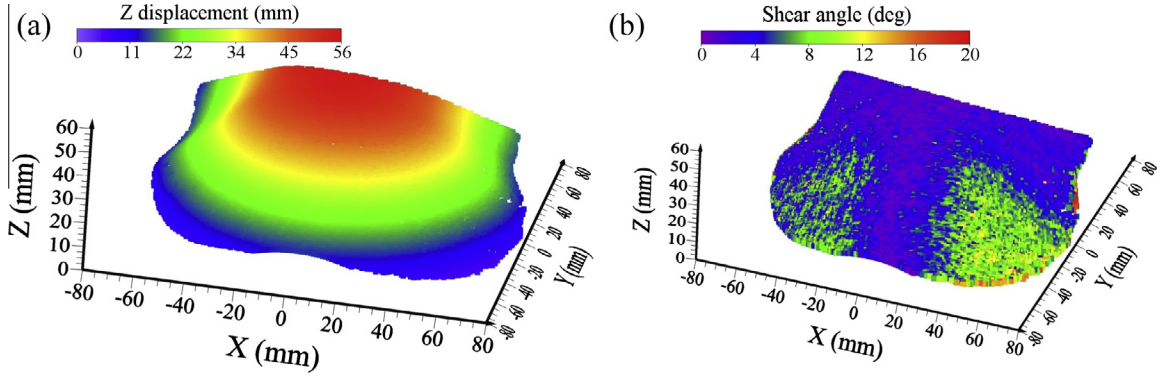


**Fig. 17.** (a) Displacement and (b) shear angle distribution at the end of forming process of double-dome shape with weft fibres in longitudinal direction.


**Fig. 18.** Deformed shape at the end of forming process of double-dome shape with (a) warp fibres and (b) weft fibres in longitudinal direction.

presented in [25] and adopted for a 3D E-glass reinforcement in [6]. The grid consists of facets, made by spacing of points (i.e. step size in pixels), in the Area of Interest (AoI) analysed during the dig-ital image correlation. The adopted step size is 5 pixels. For each recorded incremental position of the mould, DIC analysis by MatchID3D provides the 3D displacement in the field of view of the cameras as coordinates of the facets vertexes (see Figs. 16a and 17a). The post-processing of these data allows evaluation of the local shear angle as variation of the angle between the diagonals of each facet.

The distributions of the shear angle on the reinforcement's external surface at the end of the double-dome shape forming are depicted in Figs. 16b and 17b for a sample with warp yarns and weft yarns initially in the direction of the longer side of the die, respectively.

For both orientations, the higher values of shear angle are in the higher curvature zones as observed for other reinforcement fabrics (see e.g. [44,6]). The maximum shear angle does not exceed 14° for both orientations of the reinforcement in the final shape. This is an interesting observation because the recorded maximum shear angle is lower than measured for other reinforcements. For the same double-dome shape, the 3D E-glass reinforcement investigated in [6] has maximum shear angle close to 25° while the twill 2/2 glass-PP fabric adopted in [51] has a maximum angle of 28°.

Finally, it is important to underline that the quasi-unidirectional flax reinforcement does not feature relevant defects (e.g. wrinkles or openings) during the double-dome forming for both the considered initial orientations of the yarns (Fig. 18). The observed good drapability of the flax fabric is mainly related to its architecture with a reduced number of intersections leading

to a reduced influence of the friction in the initial shear deformation, one of the primary deformation mechanisms in a reinforcement shaping.

It should be mentioned that the considered double-dome is not one of the most complex 3D shapes. For a wider assessment of the formability of the flax fabric other more severe 3D shapes (e.g. tetrahedron) will be considered.

## 6. Conclusions

The experimental study presented in this paper was focused on understanding the deformability and formability of a quasi-unidirectional flax reinforcement for composite materials, commercialized as FLAXPLY UD 180 by LINEO.

The first part was focused on the main deformation modes of the flax fabric. The main results of the investigation are:

- The biaxial tensile tests, performed for different velocity ratios *k*, provided a complete understanding of the biaxial behaviour of the reinforcement. The fabric stiffness per yarn in the warp direction at strain over 0.5% for biaxial test and 1% for uniaxial test is close to the stiffness of individual flax yarn.
- The uniaxial bias extension and picture frame tests provide very similar shear behaviour of the fabric and show good agreement with theoretical models.
- The out-of-plane bending tests feature a completely different bending behaviour in warp and weft direction of the fabric, due to the difference in yarn density.
- The out-of-plane compression tests show the variation of the fabric thickness when increasing the transverse pressure as in the compaction stage of resin infusion processes. The response of the reinforcement in terms of thickness variation allows the preliminary prediction of the fibre content in the composite and, as consequence, of the mechanical performance.

The second part of this study was dedicated to the experimental simulation of a complex 3D shape forming process using a double-dome punch. The main results are:

- Experimental observations showed a shear angle distribution on the fabric surface similar to other reinforcements at the end of the shaping process. Moreover, the maximum shear angle measured on the quasi-UD flax fabric is definitively lower than that observed for other reinforcements. The relatively low shear angles generated in complex shape forming indicate the very good drapability of the adopted flax fabric.
- The peculiar properties of the quasi-unidirectional flax reinforcement are appropriate to generate the considered complex shape without visible defects.

The obtained results represent a complete and unique data set for the knowledge of the deformation capabilities during complex 3D shape forming processes with the considered quasi-unidirectional flax reinforcement for composite materials. Moreover, the measurements obtained during experimental double-dome shaping allow increasing the confidence in adopting the flax fibre quasi-UD reinforcement in forming complex composite components and assessing the accuracy of available predictive models.

## Acknowledgements

LINEO is acknowledged for manufacturing and supplying the quasi-unidirectional flax reinforcement (FLAXPLY UD 180). The research has been carried out in the framework of the Erasmus Master program of Bart Vanleeuw in Politecnico di Milano and K.U. Leuven. The work of Marcin Barburski was funded by the Polish Ministry of Science and High Education (grant 631/MOB/2011). The help of laboratory staff of the KU Leuven Department MTM – Bart Pelgrims and Kris Van de Staey – is gratefully acknowledged. The support and help in DIC computations with MatchID3D of Bart Van Mieghem is gratefully acknowledged. Authors are grateful to Phillippe Boisse (INSA Lyon) for discussions on the flax fabric behaviour.

## References

[1] Long AC. Composites forming technologies. Woodhead Publishing Limited; 2007.
[2] Boisse P. Composite reinforcements for optimum performance. Oxford: Woodhead Publishing Limited; 2011.
[3] Charmetant A, Orliac JG, Vidal-Sallè E, Boisse P. Hyperelastic model for large deformation analyses of 3D interlock composite preforms. Compos Sci Technol 2012;72:1352–60.
[4] De Luycker E, Morestin F, Boisse P, Marsal D. Simulation of 3D interlock composite preforming. Compos Struct 2009;88:615–23.
[5] Carvelli V, Pazmino J, Lomov SV, Verpoest I. Deformability of a non-crimp 3D orthogonal weave E-glass composite reinforcement. Compos Sci Technol 2012;73:9–18.
[6] Pazmino J, Carvelli V, Lomov SV. Formability of a non-crimp 3D orthogonal weave E-glass composite reinforcement. Composites: Part A 2014;61:76–83.
[7] Wambua P, Ivens J, Verpoest I. Natural fibres: can they replace glass in fibre reinforced plastics? Compos Sci Technol 2003;63:1259–64.
[8] Maya JJ, Sabu T. Biofibres and biocomposites. Carbohydr Polym 2008;71:343–64.
[9] La Mantia FP, Morreale M. Green composites: a brief review. Composites: Part A 2011;42:579–88.
[10] Yan L, Chouw N, Jayaraman K. Flax fibre and its composites – a review. Composites: Part B 2014;56:296–317.
[11] Faruka O, Bledzkia AK, Fink HP, Sain M. Biocomposites reinforced with natural fibers: 2000–2010. Progr Polym Sci 2012;37:1552–96.
[12] Defoirdt N, Biswas S, De Vriese L, Quan Ngoc Tran L, Van Acker J, Ahsan Q, et al. Assessment of the tensile properties of coir, bamboo and jute fibre. Composites Part A 2010;41:588–95.
[13] Trujillo E, Moesen M, Osorio L, Van Vuure AW, Ivens J, Verpoest I. Bamboo fibres for reinforcement in composite materials: strength Weibull analysis. Composites Part A 2014;61:115–25.
[14] Dittenber DB, GangaRao HV. Critical review of recent publications on use of natural composites in infrastructure. Composites: Part A 2012;43:1419–29.
[15] Ouagne P, Soulat D, Tephany C, Duriatti D, Allaouie S, Hivet G. Mechanical characterisation of flax-based woven fabrics and in situ measurements of tow tensile strain during the shape forming. J Compos Mater 2013;47:3501–15.
[16] Ouagne P, Soulat D, Moothoo J, Capelle E, Gueret S. Complex shape forming of a flax woven fabric; analysis of the tow buckling and misalignment defect. Composites: Part A 2013;51:1–10.
[17] Capelle E, Ouagne P, Soulat D, Duriatti D. Complex shape forming of flax woven fabrics: design of specific blank-holder shapes to prevent defects. Composites: Part B 2014;62:29–36.
[18] Boisse P, Zouari B, Daniel JL. Importance of in-plane shear rigidity in finite element analyses of woven fabric composite preforming. Composites Part A 2006;37(12):2201–12.
[19] Potluri P, Parlak I, Ramgulam R, Sagar TV. Analysis of tow deformations in textile preforms subjected to forming forces. Compos Sci Technol 2006;66:297–305.
[20] Hamila N, Boisse P, Sabourin F, Brunet M. A semi-discrete shell finite element for textile composite reinforcement forming simulation. Int J Numer Methods Eng 2009;79:1443–66.
[21] Gatouillat S, Bareggi A, Vidal-Sallé E, Boisse P. Meso modelling for composite preform shaping – simulation of the loss of cohesion of the woven fibre network. Composites: Part A 2013;54:135–44.
[22] Peng X, Ding F. Validation of a non-orthogonal constitutive model for woven composite fabrics via hemispherical stamping simulation. Compos: Part A 2011;42:400–7.
[23] Correlated Solutions, Inc., VIC-2D, Irmo, SC, USA: <http://www.correlatedsolutions.com>; 2012.
[24] Sutton MA, Orteu JJ, Shreir HW. Image correlation for shape, motion and deformation measurements: basic concepts, theory and applications. Springer Science; 2009.
[25] Lomov SV, Boisse P, Deluycker E, Morestin F, Vanclooster K, Vandepitte D, et al. Full-field strain measurements in textile deformability studies. Composites: Part A 2008;38:1232–44.
[26] Boisse P, Hamila N, Vidal-Sallè E, Dumont F. Simulation of wrinkling during textile composite reinforcement forming. Influence of tensile, in-plane shear and bending stiffnesses. Compos Sci Technol 2011;71:683–92.
[27] Nguyen QT, Vidal-Sallé E, Boisse P, Park CH, Saouab A, Bréard J, et al. Mesoscopic scale analyses of textile composite reinforcement compaction. Composites Part B 2013;44:231–41.

[28] MatchID – Image Correlation & Material Identification Mechanics of Materials, Products & Processes, <http://www.matchid.org/>.
[29] Cao J, Akkerman R, Boisse P, Chen J, Cheng HS, De Graaf EF, et al. Characterization of mechanical behaviour of woven fabrics: experimental methods and benchmark results. Composites Part A 2008;39:1037–53.
[30] Harrison P, Clifford MJ, Long AC. Shear characterization of viscous woven textile composites: a comparison between picture frame and bias extension experiments. Compos Sci Technol 2004;64:1454–65.
[31] Launay J, Hivet G, Duong AV, Boisse P. Experimental analysis of the influence of tensions on in plane shear behaviour of woven reinforcements composites. Compos Sci Technol 2008;68:506–15.
[32] Lee W, Padvoiskis J, Cao J, De Luycker E, Boisse P, Morestin F, et al. Bias extension of woven composite fabrics. Int J Mater Form 2008;1:895–8.
[33] Lomov SV, Willems A, Verpoest I, Zhu Y, Barbuski M, Stoilova Tz. Picture frame test of woven composite reinforcements with a full-field strain registration. Textile Res J 2006;76(3):243–52.
[34] Lebrun G, Bureau MN, Denault J. Evaluation of bias-extension and picture frame test methods for the measurement of intraply shear properties of PP/glass commingled fabrics. Compos Struct 2003;61:341–52.
[35] Harrison P, Clifford M. Rheological behaviour of pre-impregnated textile composites. In: Design and manufacturing of textile composites. Woodhead; 2005.
[36] Zouari B, Daniel JL, Boisse P. A woven reinforcement forming simulation method. Influence of the shear stiffness. Comput Struct 2006;84:351–63.
[37] Gereke T, Döbrich O, Hübner M, Cherif C. Experimental and computational composite textile reinforcement forming: a review. Composites Part A 2013;46:1–10.
[38] Peirce F. The geometry of cloth structure. J Text Inst 1937;28:45–96.
[39] ASTM. D1388-08, Standard test method for stiffness of fabrics. West Conshohocken, PA: American Society for Testing and Materials; 2012.
[40] Lomov SV, Verpoest I, Barburski M, Laperre J. Carbon composites based on multiaxial multiply stitched preforms. Part 2. KES-F characterisation of the deformability of the preforms at low loads. Composites Part A 2003;34(4):359–70.
[41] de Bilbao E, Soulat D, Hivet G, Gasser A. Experimental study of bending behaviour of reinforcements. Exp Mech 2010;50:333–51.
[42] Lomov S, Barburski M, Stoilova T, Verpoest I, Akkerman R, Loendersloot R, et al. Carbon composites based on multiaxial multiply stitched preforms. Part 3: biaxial tension, picture frame and compression tests of the preforms. Composites: Part A 2005;36:1188–206.
[43] Sargent J, Chen J, Sherwood J, Cao J, Boisse P, Willems A, et al. Benchmark study of finite element models for simulating the thermostamping of woven-fabric reinforced composites. Int J Mater Forming 2010;3(1):683–6.
[44] Harrison P, Gomes R, Curado-Correia N. Press forming a 0/90 cross-ply advanced thermoplastic composite using the double-dome benchmark geometry. Composites: Part A 2013;54:56–69.
[45] Lomov SV, Truong Chi T, Verpoest I, Peeters T, Roose V, Boisse P, et al. Mathematical modeling of internal geometry and deformability of woven preforms. Int J Forming Proc 2003;6:413–42.
[46] Grosberg P, Park BJ. The mechanical properties of woven fabrics. Part V. The initial modulus and the frictional restraint in shearing of plain woven fabrics. Textile Res J 1966;36(5):420–31.
[47] Chen B, Chou TW. Compaction of woven-fabric preforms in liquid composite molding processes: single-layer deformation. Compos Sci Technol 1999;59:1519–26.
[48] Lomov SV, Verpoest I. Compression of woven reinforcements: a mathematical model. J Reinf Plast Compos 2000;19(16):1329–50.
[49] Kersani M, Lomov SV, Van Vuure AW, Bouabdallah A, Verpoest I. Damage in flax/epoxy quasi unidirectional woven laminates under quasi-static tension. J Compos Mater 2014, in press. doi: http://dx.doi.org/10.1177/0021998313519282.
[50] Shah DU, Porter D, Vollrath F. Opportunities for silk textiles in reinforced biocomposites: studying through-thickness compaction behaviour. Composites: Part A 2014;62:1–10.
[51] Willems A. Forming simulation of textile reinforced shell structures – PhD. Thesis, Katholieke Universiteit Leuven, ISBN 978-94-6018-009-5; 2008.